<u>THE ZEUS EXPERIMENT AT HERA.</u>

Proposal 760

Bristol, Glasgow, Imperial College London, University College London, Oxford, Rutherford Appleton Laboratory
in collaboration with
Argonne, Bologna, Bonn, Calabria, Chonnan, Columbia, DESY, DESY-Zeuthen, Florence, Frascati, Freiburg, Hamburg, Iowa, Jülich, KEK, Krakow, Kyungpook, Madison (Wisconsin), Madrid, McGill, Moscow, NIKHEF, Ohio, Padova, Pennsylvania, Rome, Santa Cruz, Seoul, Siegen, Tel Aviv, Tokyo, Tokyo Metropolitan Univ., Torino, Toronto, Warsaw, Weizmann Inst., Yale, Yokohama, York (Ontario).

1 Introduction

When HERA restarted in January 1999 after a short shutdown over Christmas, it continued e^- running from 1998 but with a much better understanding of the HERA machine. After the April - July shutdown, it was decided to restart with e^+ running and this will continue, at least initially, into the year 2000. The total e^- (e^+) luminosity delivered by HERA was 18pb^{-1} (27pb^{-1}) of which ZEUS wrote 13pb^{-1} (20pb^{-1}) to tape. The ZEUS data-taking efficiency for both e^- and e^+ was in excess of 80%, which represents a considerable improvement over 1998.

The UK groups continued to take a large share of the responsibility in data-taking, yet again providing two of the four run coordinators in 1999, as well as a good proportion of the designated shift leaders (4 units) and deputy shift leaders (3 units). In addition, the ZEUS spokesman is a UK physicist and the UK provides the ZEUS tracking coordinator, the CTD coordinator, joint coordinators for three of the five physics groups, the ZEUS analysis coordinator (until July 1999) and the ZEUS Monte Carlo code manager. A UK physicist also acted as ZEUS finance officer for the three years 1997-99. Finally, a UK PhD student became the first recipient of the newly established Björn Wiik Scholarship.

The ZEUS experiment continues to operate well and we look forward to increased luminosity from the HERA upgrades which will be installed in the shutdown beginning in September 2000. The new Microvertex detector, in which the UK is playing a significant role, and the Straw Tube Tracker, which will improve the forward tracking, will be installed in the shutdown.

2 Status of the new ZEUS Microvertex Detector (MVD)

2.1 MVD Electronics

The UCL group is designing and building the clock and control system for the MVD. The Masterbox and Slave systems, which interface between the ADCs, the global first level trigger system and the HELIX driver, have been prototyped and designed. The final boards are now being commissioned at UCL. For the HELIX driver the analogue current driver has now been designed and protyped, and digital electronics has been prototyped on a seperate board. Design and test work is continuing.

Cabling and installation are major challenges, which impinge strongly on the electronics (analogue readout as well as clock and control). A UK technician is overall coordinator for ZEUS MVD cabling issues, and we are building the patch box which will sit just beyond the rear of the MVD.

We are participating in design and feasibility studies for a combined CTD/MVD second level trigger.

2.2 ZEUS MVD Alignment

Oxford is responsible for providing the optical alignment system and later the offline alignment. The optical alignment system is a development of the technique using a laserbeam and transparent amorphous silicon diodes pioneered by the ATLAS group at MPI Munich. For ZEUS we have reduced the size of the sensors and increased the laser wavelength from the optical to the IR to optimise the transparency. At present we are using a modification of the Munich readout electronics, but in the final ZEUS system a custom ASIC will give a direct interface to VME. The development work is being led by Walczak, with Matsushita and Boogert and technical support from Hill (Design Office), Shield and Dawson (electronics). The MVD will be assembled at NIKHEF, where the MVD support tube and installation frame have been constructed and assembled. In December 1999 Dawson, Boogert and Matsushita tested the alignment system at NIKHEF. Valuable practical experience was obtained and data taken with two laser beams each with 6 sensors mounted at the ends and on the 4 flanges of the MVD support tube. From online output distortions of the structure at the level of 100 microns were measured. Better resolution is expected when the full data sample is analysed offline. One of the challenges of the MVD optical sensor readout was to make a thin, flat, low impedance, low density, non-PVC cable up to 20 m in length. Band (photographic unit) and Shield produced a very ingenious solution based on photochemical etching of a very flexible but thin copper sheet. The cable tracks are laid down on a $1 \times 0.5\,\mathrm{m}^2$ area and then cut and folded to produce cable of the required length. Sufficient cable has been produced but not yet cut to the final lengths. Installation of the optical system is expected to take place in early Spring 2000.

On the offline side Sutton has produced a parameterisation of the shapes of the MVD silicon wafers from data measured by our colleagues at DESY during acceptance tests. He has also looked into various aspects of the Monte Carlo simulation of the MVD. Once the MC code is stable work will start on identifying track samples for alignment and on the procedures to be used.

2.3 MVD Installation Plans

The UK have the responsibility for installing the MicroVertex Detector (MVD) and Beam Pipe as an assembly into the Zeus experiment. This is currently scheduled to take place towards the end of 2000.

Great familiarity with both new and existing apparatus in and around the central region of the ZEUS experiment is necessary. This includes the new beam-pipe, magnet systems and the MVD itself as well as existing detectors, the Central Tracking Detector (CTD), which was designed and built by UK groups, and other tracking chambers and calorimeters.

The installation procedure and method has evolved over the past year during which there has been dialogue between the UK installation team, the MVD mechanical designers (NIKHEF), the Beam Pipe designers (DESY) and all relevant experts. The UK team consists of three people working (part time) on installation, one with overall responsibility from the Rutherford Appleton Laboratory, and two from Oxford Nuclear Physics Dept where the detailed design and manufacture of the required hardware is being undertaken.

Early in the ZEUS upgrade schedule measurements will be made on the CTD to confirm that the proposed installation procedure can take place safely. There is an alternative procedure which will be used if necessary. Before shipment to DESY all installation hardware will have been tested on a mock-up to verify its capability and to enable us to practice the procedures.

3 CTD performance

The Central Tracking Detector (CTD), together with its associated readout and trigger electronics, is the major contribution made by the UK groups to the ZEUS detector. It remains our joint task to operate it effectively and obtain optimum results from it. The CTD is an essential component of almost all ZEUS triggers and of all ZEUS physics analyses.

The CTD continued to perform reliably during 1999 data-taking. The chamber efficiency and resolution remained satisfactory and stable. There were some operational problems with the high voltage in the latter part of the running period which are still under investigation, but no significant amount of data was lost. The CTD online computers in the experiment hall were replaced at the end of the year with new systems that are Y2K compliant. The transition to these new systems was problem free and the CTD took data using them for the last month of running.

The day-to-day operation of the CTD has been very smooth. The off-line data-quality monitoring procedures have worked very well. As part of a general ZEUS effort, we are also implementing data-quality checks online. These new procedures will ensure the quality of the CTD data for the forseeable future.

4 Physics analyses

During 1999 18 ZEUS analyses were published or submitted for publication ([1]-[18]) by various journals, of which six were originally submitted in 1998. In the following summary, we concentrate as usual on those physics areas where the UK members of ZEUS have been particularly active.

4.1 High Q^2 Neutral, Charged Current Physics and Structure Function Measurements

ZEUS UK physicists have continued their leading role in the study of high Q^2 physics at HERA. In 1998 HERA switched to running with electrons until the the end of May 1999, delivering a luminosity of $16\,\mathrm{pb}^{-1}$. This allows for the first time a high statistics measurement of the $e^- p$ high Q^2 Deep Inelastic scattering Neutral Current (NC) and Charged Current (CC) cross sections. This will permit the first comparison of the charge dependence of the NC cross section at high Q^2, showing the sensitivity to the contribution of Z^0 exchange. A preliminary analysis of the electron data up to the end of running in May 1999 has been presented was presented at the 1999 summer conferences. Figure 1 shows the neutral current differential cross section $d\sigma/dQ^2$ as a function of Q^2 for both electron and positron beams, also compared re the predictions from the standard model using CTEQ4D parton densities. Figure 2 shows the differential cross section $d\sigma/dx$ for e^-p scattering for $Q^2 > 800\,\mathrm{GeV}^2$ and in figure 3 $d\sigma/dx$ for $Q^2 > 10\,000\,\mathrm{GeV}^2$. The effect of the positive interference of the photon γ and Z^0 can be clearly seen in the electron data from figure 3. The new high statistics electron data in combination with previous and forth coming positron data permits the first extraction of the proton structure function xF_3, a measurement which is currently in progress.

Last year ZEUS published results on the CC cross section for e^+p DIS using the 1994-1997 data. The publication contains the single and double differential cross sections. The double differential cross section is shown at fixed Q^2 as a function of x in figure 5. Since the W-boson is charged, the CC picks out specific quark flavours from the proton. The CC in e^+p scattering is sensitive to the d-quark density, particularly at high x. Since, at present, the d-quark density is less well known than that of the u-quark these data will be of great importance in constraining parameterisations of proton structure. In addition, the paper contains a determination of the mass of the W-boson and a detailed confrontation of the data with the Standard Model.

The analysis of the 16 pb^{-1} of e^-p data is now well under way. Preliminary results were presented from a subset of the data at the spring and summer conferences of 1999. The objective now is to extract single and double differential cross sections from the full data set. These data will then be used to investigate in detail the dependence of the CC cross section on the charge of the lepton beam which is indicated in figure 4.

4.1.1 Structure Function Measurements

ZEUS UK physicists have continued their leading role in structure function measurements during the past year the extraction of F_2 from initial state radiation events collected during 1996/97, a particularly difficult measurement. ZEUS UK physicists have been involved in the main analysis team for the extraction of F_2 over the same period and in F_2 phenomenology with contributions to QCD and electroweak fitting of the extracted high Q^2 structure functions, with the goal of extracting the maximum amount of information from the NC and CC structure functions.

Further investigations into the hadronic final state of events with high transverse momentum (high E_T) have been performed, with the first analysis of W production and isolated high p_T leptons [8]. The later subject is controversial as H1 have seen more events of this type particularly in the muon channel, than the Standard Model predicts. So far ZEUS finds events at a rate in agreement with the SM. The analysis of this channel has be continued for the 1998/99 electron data. Other analyses in progress are investigations of high jet events with very high total E_T, of particular interest is their flavour content as any anomalous flavour content could indicate new physics.

4.1.2 Charm Production in Deep Inelastic Scattering

In Deep Inelastic Scattering (DIS) charm is produced predominantly through the boson-gluon fusion mechanism. Charm events are identified by reconstructing D^* mesons via their decays $D \rightarrow D^0\pi_s$, $D^0 \rightarrow K\pi$ and $D^0 \rightarrow K\pi\pi\pi$. Differential cross sections and F_2^{charm} were measured using both decay modes from the combined 1996-97 data sample, which corresponds to an integrated luminosity of $37\,\mathrm{pb}^{-1}$. Both the cross sections and structure function are in good agreement with next-to-leading order QCD predictions. These final results were accepted for publication at the end of last year [14] and are shown in figures 6 and 7. There is evidence for fragmentation effects "pulling" the D_s^* towards the direction of the proton remnant as shown in figure 6, but the effect is modeled reasonably well by Monte Carlo fragmentation models and has a negligible effect on the final extraction of the structure function.

4.2 Charm Production in Diffractive Scattering

Charm production in diffractive interactions is particularly important due to its sensitivity to the presence of gluons. Hence it is a powerful tool to distinguish between different theoretical models of diffraction. The principle interactions of interest are photon dissociative reactions (in which the photon dissociates into a hadronic system while the proton remains intact). These events can be identified by the presence of a rapidity gap between the hadronic system and the outgoing proton direction. As in DIS, charm was identified using D* reconstruction and events were only identified as diffractive if the measured rapidity gap was at least 1.75 units. Differential D^* cross sections have been measured using the combined 1995-97 data sample for the $D^0 \rightarrow K\pi$ decay and the 1996-97 data for the $D^0 \rightarrow K\pi\pi\pi$ channel. The ratio of diffractive charm production to DIS charm was also determined. These preliminary results were presented at the summer conferences and are shown in figures 8, 9 and 10.

4.3 Jet Production

Studies of jets in photon-proton collisions at HERA continue to give information on the hadronic "structure" of the photon. In 1999 we measured the dynamics of three jet production, showing explicitly the effects of the colour of the incoming quarks and gluons, a fundamental test of the strong interaction as shown in figure 11. ZEUS UK physicists are currently working on the high statistics sample of data which ZEUS has now assembled, which will give information on photon structure at higher scales than achieved anywhere before.

4.4 Charm and Beauty Production

Charm and beauty quarks inside jets using D^* were measured in 1998 and published in 1999 [4]. We measured charm production by detecting the decays of D^* hadrons which contain charm quarks. The results showed for the first time that charm is produced copiously in those types of event where the photon fluctuates into a hadronic system ("resolved photon" events). Heavy quarks can also be detected by identifying electrons from their decay. This is done by measuring the distinctive rate of energy loss of electrons in the CTD, as well as the way they interact in the calorimeter. Preliminary results from this method not only confirm the result of the D^* studies, but also show a significant production rate for beauty quarks shown in figure 12. Understanding such results is an important test of QCD and a necessary step towards understanding the new physics potential of future colliders.

4.5 Hadronic Final States

Semi-inclusive processes in deep inelastic scattering (DIS) are of importance because they can be used to test the perturbative Quantum Chromodynamics (QCD) description of hadron production via parton fragmentation. An observable of particular interest is the distribution of the azimuthal angle, ϕ, (measured in the hadronic centre-of-mass frame) between the lepton scattering plane, defined by the incoming and outgoing lepton momenta, and the hadron production plane, defined by the incoming virtual boson and an outgoing hadron, see figure 13.

Asymmetries in the ϕ distribution, i.e. terms proportional to $\cos\phi$ and $\cos 2\phi$, are expected from both non-perturbative and perturbative effects (e.g. refs. [35, 36, 37, 38, 39, 40]). The non-perturbative asymmetry results from the intrinsic momentum of a quark in the proton. Since the intrinsic momentum is small, this asymmetry falls rapidly with increasing transverse momentum of the measured hadron and with increasing Q^2, the virtuality of the exchanged boson [36]. In contrast, the perturbatively induced asymmetry is only weakly dependent on Q^2 and persists at high hadron transverse momenta. To leading order (LO) in α_s two processes contribute to DIS: QCD-Compton scattering (QCDC, $\gamma^* q \to qg$) and boson-gluon fusion (BGF, $\gamma^* g \to q\bar{q}$). For the QCDC process the scattered quark tends to appear at ϕ near 180° whilst for the BGF process the ϕ dependence has a symmetry that $\phi \leftrightarrow 180° - \phi$, as a consequence of a quark and an anti-quark being present in the final state.

Figure 14 shows the moments $\langle\cos\phi\rangle$ and $\langle\cos 2\phi\rangle$ as a function of the minimum transverse momentum of the charged hadron, p_c. The statistical errors are those obtained from fitting the data. The value of $\langle\cos\phi\rangle$ is negative and decreases in magnitude from ≈ -0.08 to ≈ -0.03 as p_c is increased. Although a contribution is predicted also from non-perturbative effects, a negative value is expected for a vector gluon in contrast to a positive value expected for a scalar gluon [39]. The reduction with increasing p_c is consistent with the expectation from BGF processes which would give a positive $\langle\cos\phi\rangle$ at high p_c in contrast to the negative contribution from QCDC. The value of $\langle\cos 2\phi\rangle$ is positive. It rises, at low p_c, from a value consistent with zero to ≈ 0.09 as p_c is increased to 2.0 GeV/c; this is to be expected from the dominance of BGF over QCDC at high transverse momenta.

Figure 14 also compares the data with two LO QCD calculations. Both calculations were made with Q as the appropriate scale, with the Binnewies et al. LO fragmentation function [41] and the CTEQ4 LO proton parton densities [42]. The Ahmed-Gehrmann calculation [40] is purely at $\mathcal{O}(\alpha_s)$ whilst the calculation from ZEUS (based on [39]) includes an estimation of the non-perturbative contribution. In addition, the results of Ahmed-Gehrmann are calculated at the mean values $\langle x \rangle$ and $\langle Q^2 \rangle$, whilst the calculation from ZEUS integrates over the kinematic range. These different implementations account for the observed difference in the two predictions; using $\langle x \rangle$ and $\langle Q^2 \rangle$in the ZEUS perturbative calculation leads to agreement with the Ahmed-Gehrmann calculation. The non-perturbative contribution to the calculation is at most 20% at low p_c for $\langle \cos\phi \rangle$ for a mean intrinsic k_t of 0.5 GeV/c and a non-perturbative fragmentation p_t of 0.5 GeV/c. This fraction depends though on the parameters used. On the other hand this non-perturbative contribution is negligible for $\langle \cos 2\phi \rangle$. From this it can be concluded that the observation of a significant $\langle \cos 2\phi \rangle$ term is clear evidence for a perturbative contribution to the azimuthal asymmetry.

The sensitivity to higher order corrections was examined at the partonic level using the DISENT Monte Carlo program [43]. This suggests that higher-order corrections are large (factors of 2-3) at low p_c for the $\langle \cos\phi \rangle$ term, resulting in larger negative values; for the $\langle \cos 2\phi \rangle$ term they are much smaller. This may explain the disagreement between the data and the LO QCD models for $\langle \cos\phi \rangle$ at low p_c.

The azimuthal asymmetry in the deep inelastic electroproduction of single particles has been measured at HERA in the hadronic centre-of-mass frame, and in a kinematic region in which perturbative QCD effects are expected to dominate. For hadrons produced at large transverse momenta the results for $\langle \cos\phi \rangle$ and $\langle \cos 2\phi \rangle$ are in agreement with QCD predictions. The measured value of $\langle \cos\phi \rangle$ is negative and compatible with that expected for a vector gluon. The moment $\langle \cos 2\phi \rangle$, which is measured for the first time, is shown to be non-zero and positive. It increases as a function of the minimum particle transverse momentum, in agreement with predictions containing a dominant contribution from boson-gluon fusion. This provides clear evidence for a perturbative QCD contribution to the azimuthal asymmetry.

4.5.1 Modified leading log comparison

The fragmentation of the struck quark in DIS is compared to that of the quarks produced in e^+e^- annihilation, allowing the concept of universality of fragmentation to be tested. A comparison is also made of the fragmentation associated with the outgoing struck quark to that in the target region; the latter is associated with the initial state radiation from the incoming proton. The data are compared to analytical Quantum Chromodynamic (QCD) predictions for the momenta spectra for both the current and target region.

A natural frame in which to study the dynamics of the hadronic final state in DIS is the Breit frame [25]. In this frame, the exchanged virtual boson (γ^*) is completely space-like and has a four-momentum $q = (0, 0, 0, -Q = -2xP^{Breit}) \equiv (E,\ p_x,\ p_y,\ p_z)$, where P^{Breit} is the momentum of the proton in the Breit frame. The particles produced in the interaction can be assigned to one of two regions: the current region if their z-momentum in the Breit frame is negative, and the target region if their z-momentum is positive. The main advantage of this frame is that it gives a maximal separation of the incoming and outgoing partons in the QPM. In this model the maximum momentum a particle can have in the current region is $Q/2$, while in the target region the maximum is $Q(1-x)/2x$. In the Breit frame, unlike the hadronic centre of mass ($\gamma^* p$) frame, the two regions are asymmetric, particularly at low x, where the target region occupies most of the available phase space.

The current region in the ep Breit frame is analogous to a single hemisphere of e^+e^- annihilation. In $e^+e^- \to q\bar{q}$ annihilation the two quarks are produced with equal and opposite momenta, $\pm\sqrt{s_{ee}}/2$. The fragmentation of these quarks can be compared to that of the quark struck from the proton; this quark has an outgoing momentum $-Q/2$ in the Breit frame. In the direction of this struck quark the scaled momentum spectra of the particles, expressed in terms of $x_p = 2p^{Breit}/Q$, are expected to have a dependence on Q similar to that observed in e^+e^- annihilation [26, 27, 28] at energy $\sqrt{s_{ee}} = Q$.

Within the framework of the modified leading log approximation (MLLA) there are predictions of how the higher order moments of the parton momentum spectra should evolve with the energy scale [29, 30]. The MLLA calculations are made at the parton level. The hypothesis of local parton hadron duality (LPHD) [31], which relates the observed hadron distributions to the calculated parton distributions via a constant of proportionality, is used in conjunction with the parton predictions of the MLLA to allow the calculation to be directly compared to data.

DIS at low x allows a study of fragmentation in the target region following the initial scattering off a sea quark (or anti-quark). The description based on MLLA [32] is shown schematically in figure 15, where the quark box at the top of the gluon ladder represents the scattered sea quark plus its anti-quark partner. There are various contributions to these calculations. Contribution C, the top leg of the quark box, corresponds to fragmentation in the current region. Three further contributions (T1, T2 and T3), which are sources of soft gluons, are considered in these analytical calculations to be associated with the target region. It is predicted [32] that the contribution T1 behaves in the same way as the current quark C and so should have no x dependence. The contribution T2 is due to the colour field between the remnant and the struck quark, and the contribution T3 corresponds to the fragmentation of the rungs in the gluon ladder. Both T2 and T3 are predicted to have x and Q^2 dependences which differ from T1. Both the T1 and T2 contributions have been calculated and give particles of momenta $< Q/2$. The collinear gluons T3, on the other hand, generally fragment to particles with momentum $\gtrsim Q/2$. For values of the scaled momentum $x_p < 1.0$, the region of phase space is analogous to the current region and has contributions mainly from T1 and T2. The parton momentum spectra predicted by MLLA, over a range of Q^2 and x, are shown in more detail in [27]. In the target region these spectra are approximately Gaussian for $x_p < 1$; they peak at a value of $x_p \sim 0.1 - 0.2$ in the range of x and Q^2 measured in this paper, falling to a plateau region for $1 < x_p < (1-x)/x$ (the maximum value of x_p in the target region). The acceptance of the ZEUS detector allows the study of the contributions from C, from T1 and from T2.

4.5.2 Current fragmentation region

Figure 16 shows the moments of the $\ln(1/x_p)$ spectra as a function of Q^2. It is evident that the mean and width increase with increasing Q^2, whereas the skewness and kurtosis decrease. Similar fits performed on e^+e^- data [33] show a reasonable agreement with our results, consistent with the universality of fragmentation for this distribution.

The data are compared to the MLLA predictions of [30], using a value of $\Lambda = 175$ MeV, for different values of Q_0. A comparison is also made with the predictions of [29] for the limiting spectrum ($Q_0 = \Lambda$). The MLLA predictions of the limiting spectrum in [30] describe the mean well. However both of the MLLA calculations predict a negative skewness which tends towards zero with increasing Q^2 in the case of the limiting spectra. This is contrary to the measurements. The qualitative description of the behaviour of the skewness with Q^2 can be achieved for a truncated cascade ($Q_0 > \Lambda$), but a consistent description of the mean, width, skewness and kurtosis cannot be achieved. A range of Λ values was investigated and no single value of Λ gave a consistent description of all the moments.

We conclude that the MLLA predictions, assuming LPHD, do not describe the data.

4.5.3 Target fragmentation region

The distributions of charged particles in x_p in the target region of the Breit frame are studied as a function of x and Q^2, in the range $6 \times 10^{-4} < x < 1 \times 10^{-2}$ and $10 < Q^2 < 320$ GeV^2. This analysis is restricted to values of the scaled momenta $x_p < 1.0$ so that similar phase space regions for the target and current can be compared. Thus the accepted part of the target region corresponds to the contributions T1 and T2 in figure 15 and is only a small part of the complete phase space.

The distributions in $\ln(1/x_p)$ are shown for both the target and current regions in figure 17. The fitted curves shown are two-piece normal distributions [34] to guide the eye. In contrast to the current region, the target region distribution does not fall to zero as $\ln(1/x_p)$ tends to zero. Although the magnitude of the single particle density at the peak position of the current region distribution grows by a factor of about three over the Q^2 range shown, the single particle density of the target distribution, at the x_p value corresponding to the peak of the current distribution (contribution C is equivalent to contribution T1 in figure 15), depends less strongly on Q^2 and increases by only about 30%. In addition the $\ln(1/x_p)$ distribution shows no significant dependence on x when Q^2 is kept constant. In the target region the peak position of the $\ln(1/x_p)$ distribution increases more rapidly with Q^2 than in the current region; this is consistent with the behaviour expected from cylindrical phase space. The approximate Gaussian distribution of the MLLA predictions peaking at $\ln(1/x_p) \sim 1.5 - 2.5$ [27] is not observed. We conclude that the target distributions are inconsistent with the MLLA predictions when used in conjunction with LPHD.

4.5.4 Summary

Charged particle distributions have been studied in the Breit frame in DIS over a wide range of Q^2. The distributions in scaled momentum, x_p, have been measured for the first time in the target region of the Breit frame for $1.2 \times 10^{-3} < x < 1 \times 10^{-2}$ and $10 < Q^2 < 320$ GeV^2.

In the current region, the results show clear support the hypothesis of the coherent nature of QCD cascades. The comparison of our results in the current region of the Breit frame with e^+e^- data at $Q^2 = s_{ee}$ for $Q^2 > 80$ GeV^2 shows good agreement. The moments of the $\ln(1/x_p)$ spectra in the current region exhibit the same energy scale behaviour as those observed in e^+e^- data. The observed charged particle spectra are consistent with the universality of quark fragmentation in e^+e^- and DIS at high Q^2. The moments cannot be described by the MLLA calculations together with LPHD.

The target region $\ln(1/x_p)$ distribution shows a weaker Q^2 dependence than the corresponding current region distribution. In particular, the magnitude of the single particle density of the target distribution, at the x_p value corresponding to the peak of the current distribution, increases by about 30%, in contrast to a threefold increase for the current region in the Q^2-range considered here. The MLLA predictions for the target region, in conjunction with LPHD, fail to describe the data.

4.6 Measurement of inclusive prompt photon photoproduction at HERA

When electrons or positrons collide with protons at HERA, most of the interactions take place by electron first radiating a photon. This then interacts with the proton, and in most cases the photons physically resemble those of ordinary light, except that they are of very much higher energy. Thus, we can "look" at the structure of the photon using "very high energy light".

Sometimes the incoming photon can scatter off quarks inside the proton and re-emerge at a high angle, where the ZEUS experiment can detect it. Emerging photons such as this are termed *prompt* photons. Thus, by this means we are even looking at the quarks inside the proton. There are other possible reactions, however, which can also give rise to prompt photons, mainly when the incoming photon itself behaves as a source of quarks and gluons. When these scatter off the quarks and gluons in the proton, prompt photons can sometimes be produced. What we observe, finally, is the sum of all these possible processes.

In figure 18, we first see the transverse component of the energy of the prompt photons observed by ZEUS. This is compared with various theoretical predictions. The second plot shows the angular distribution of the prompt photons. The quantity η^γ, known as rapidity, is an angular measure which is zero when a particle emerges at 90 degrees in the laboratory, and takes values of ±1 when the particle is seen at ±45 degrees in the laboratory (positive is in the proton direction). The two plots show that the transverse energy is well predicted on average by most of the theories, although the HERWIG [44] theory is a little low. However the observed angular distribution of the photons is higher than all the theories in the backward region. This means that the parton structure of the photon, as used in the theoretical models, may not be completely correct.

Ph.D Theses.

1. H.Blaikley, (Oxford) *Measurement of proton structure from the 1996 and 1997 radiative scattering data using the ZEUS detector.*
2. J.E.Cole, (Imperial) *Open charm production in deep inelastic diffractive ep scattering at HERA.*
3. J.K.Edmonds, (Oxford) *Measurement of the NC DIS cross section at HERA using* e^+ *data from the ZEUS detector.*
4. N.Macdonald, (Glasgow) *Structure of the virtual photon at HERA.*
5. D.Picconi, (Bristol) *A Measurement of* ρ^0 *Photoproduction in* e^+P *Collisions.*
6. M.Wing, (UCL) *The Study of Heavy Quark Production in High ET Photoproduction at HERA using the ZEUS Detector.*

Talks on ZEUS and ZEUS-related physics given at major National or International Conferences.

1. D.Bailey, *Measurement of the charm structure function of the proton*, The Structure of the Nucleon, Frascati, Italy, June 1999
2. N.Brook, *Momentum spectra in the current region of the Breit frame in deep inelastic scattering at HERA*, 3rd UK Phenomenology Workshop on HERA Physics, Durham, September 1998
3. N.Brook, *Fragmentation and Event Shapes in DIS*, New Trends in HERA Physics, Tegernsee, Germany, June 1999
4. N.Brook, T.Carli, E.Rodrigues, M.R.Sutton, N.Tobien, M.Weber, *A comparison of deep-inelastic scattering Monte Carlo event generators to HERA data*, DESY MC Workshop, Hamburg, April 1998
5. N.Brook, *MLLA parton spectra compared to ARIADNE*, DESY MC Workshop, Hamburg, April 1998

6. P.Bussey, *Photoproduction at low Q2*, Physics in Collision, Ann Arbor, 1999
7. J.M.Butterworth, *QCD: How we can help each other*, Plenary talk at UK Phenomenology Workshop on Collider Physics, 19 - 24 September 1999, St John's College, Durham, UK.
8. J.M.Butterworth, *Photon Structure*, Invited talk at Lepton-Photon 99, 18/8/99, Stanford Univ., USA.
9. J.M.Butterworth, J.Chyla, G.Schuler, *Transition from Photoproduction to DIS - Introduction and Summary*, Proceedings of HERA Monte Carlo Workshop
10. J.M.Butterworth, R.J.Taylor, *Global Comparisons of Jet Photoproduction Data and Monte Carlo*, Proceedings of HERA Monte Carlo Workshop
11. J.M.Butterworth, R.J.Taylor, *A Global Study of Photon-Induced Jet Production*, Proceedings of Photon 99, Freiburg, Germany.
12. J.E.Cole, *Diffractive D^{*+-} (2010) Production in Deep Inelastic Scattering from ZEUS*, Procedings of the 6th International Workshop on Deep Inelastic Scattering and QCD, Brussels, 4-6 April 1998, World Scientific.
13. A.M.Cooper-Sarkar et al., *High Q^2 deep inelastic scattering at HERA*, 3rd Durham Workshop on HERA Physics, Durham, Sept. 1998, J. Phys. G 25 no 7 (1999) 1387-1409
14. A.M.Cooper-Sarkar, *Structure Functions at low Q^2*, Nucleon99, Frascati, June 1999.
15. R.Devenish & W.J.Stirling, Introduction, 3rd Durham Workshop on HERA Physics, Durham, Sept. 1998, J. Phys. G 25 no 7 (1999) 1269-1272
16. R.C.E.Devenish, *Nucleon and Nuclear Structure Functions*, QCD Challenges, Kfar Giladi, Israel, June 1999.
17. A.Doyle,*Event shapes and forward jet production at HERA*, Hadron 99, Beijing, 1999
18. J. Grosse-Knetter, *NC and CC Cross Sections at High Q^2 from ZEUS at HERA*, Proc. ICHEP98, Vancouver, eds A.Astbury, D.Axen & J.Robinson, World Sci. 1999, 809
19. J.Grosse-Knetter, *DIS at high Q^2*, German Physical Society, Heidelberg, March 1999 and Blois99, July 1999.
20. Th.Hadig and G.McCance, *A common scheme for running NLO ep event generators*, DESY MC Workshop, Hamburg, April 1998
21. M.E.Hayes, *Heavy Flavours in Photoproduction at HERA*, Rencontres de Moriond on QCD and Hadronic Interactions 20-27 March 1999, Les Arcs, France
22. E.A.Heaphy, *Three-jet Production at HERA*, UK Phenomenology Workshop on Collider Physics, 19 - 24 September 1999, St John's College, Durham, UK.
23. G.D.Howell, *Measurement of the e+p Charged Current Cross Section*, Procedings of the 6th International Workshop on Deep Inelastic Scattering and QCD, Brussels, 4-6 April 1998, World Scientific.
24. J.Kalinowksi, M.W.Krasny & R.Walczak, *High E_T, exotics and rare processes – an introduction*, 3rd Durham Workshop on HERA Physics, Durham, Sept. 1998, J. Phys. G 25 no 7 (1999) 1411
25. K.R.Long, *Future ep Physics: The Outlook for HERA*, 14th International Workshop on High Energy Physics and Quantum Field Theory, Moscow, 27 May - 02 June 1999.
26. K.R.Long, *Searches for New Physics at HERA*, Invited talk at the 1st International Conference 'From the Planck Scale to the Electroweak Scale', Kazimierz, 25-29 May 1998.
27. K.R. Long, *Deep Inelastic Scattering at HERA*, Invited talk at the Institute of Physics

Nuclear and Particle Physics Conference, Salford, 12-14 April 1999.

28. N.Macdonald, *Structure of real and virtual photons from ZEUS*, DIS 99, Zeuthen, 1999
29. T.Matsushita et al., *High p_T leptons and W production at HERA*, 3rd Durham Workshop on HERA Physics, Durham, Sept. 1998, J. Phys. G 25 no 7 (1999) 1412-1417
30. T.Matsushita, E.Perez & R.Rückl, *High Q^2 physics at HERA and searches for new particles*, 3rd Durham Workshop on HERA Physics, Durham, Sept. 1998, J. Phys. G 25 no 7 (1999) 1418-1427
31. T. Matsushita, *W cross-section and events with high p_t leptons*, Moriond EW, March 1999.
32. G.McCance, *NLO program comparison for event shapes*, DESY MC Workshop, Hamburg, April 1998
33. N.McCubbin, *Low x, low Q^2 physics at HERA*, PANIC 99, Uppsala, Sweden, June 1999
34. C.Nath, R.Walczak & Y.Tamazaki, *Events with large E_T^{tot} in photoproduction at HERA*, 3rd Durham Workshop on HERA Physics, Durham, Sept. 1998, J. Phys. G 25 no 7 (1999) 1440-1443
35. A. Quadt, *Measurement and Phenomenology of the proton structure function F_2 from ZEUS at HERA*, Proc. ICHEP98, Vancouver, eds A. Astbury, D. Axen & J. Robinson, World Sci. 1999, 814
36. M.R. Sutton et al, *A Comparison of Deep Inelastic Scattering Monte Carlo Event Generators to HERA Data*, Proc. of the Workshop on Monte Carlo Generators for HERA Physics, Eds G.Grindhammer, G.Ingelman, H.Jung & T.Doyle, DESY (1999)
37. L.Sinclair (convener) et al, *Progress and problems in QCD - report from the hadronic final states working group at DIS 99*, DIS 99, Zeuthen, 1999
38. L.Sinclair, *Hard photoproduction and the structure of the photon*, Ringberg Workshop, 1999
39. D.S.Waters, *Exotic and rare processes at HERA*, 3rd Durham Workshop on HERA Physics, Durham, Sept. 1998, J. Phys. G 25 no 7 (1999) 1351-1359

References

[1] ZEUS Collaboration; J.Breitweg et al., *Measurement of Jet Shapes in High Q^2 Deep Inelastic Scattering at HERA*, DESY 98-038 (March 1998), The European Physical Journal C8 (1999) 3, 367-380.

[2] ZEUS Collaboration; J.Breitweg et al., *Forward Jet Production in Deep Inelastic Scattering at HERA*, DESY 98-050 (May 1998), The European Physical Journal C6 (1999) 239-252.

[3] ZEUS Collaboration; J.Breitweg et al., *Measurement of the Diffractive Cross Section in Deep Inelastic Scattering using ZEUS 1994 Data*, DESY 98-084 (July 1998), The European Physical Journal C6 (1999) 43-66.

[4] ZEUS Collaboration; J.Breitweg et al., *Measurement of inclusive D^{*+-} and associated dijet cross sections in photoproduction at HERA*, DESY 98-085 (July 1998), The European Physical Journal C6 (1999) 67-83.

[5] ZEUS Collaboration; J.Breitweg et al., *Exclusive Electroproduction of ρ^0 and J/ψ Mesons at HERA*, DESY 98-107 (August 1998), The European Physical Journal C6 (1999) 603-627.

[6] ZEUS Collaboration; J.Breitweg et al., *ZEUS Results on the Measurement and Phenomenology of F_2 at Low x and Low Q^2*, DESY 98-121 (September 1998), The European Physical Journal C7 (1999) 609-630.

[7] ZEUS Collaboration; J.Breitweg et al., *Measurement of Multiplicity and Momentum Spectra in the Current and Target Regions of the Breit Frame in Deep Inelastic Scattering at HERA*, DESY 99-041 (March 1999), The European Physical Journal C 11 (1999) 2, 251-270.

[8] ZEUS Collaboration; J.Breitweg et al., *W Production and the Search for Events with an Isolated High-Energy Lepton and Missing Transverse Momentum at HERA*, DESY 99-054 (July 1999), accepted by Physics Letters B - WI 5040.

[9] ZEUS Collaboration; J.Breitweg et al., *Measurement of High Q^2 Neutral Current e+p Deep Inelastic Scattering Cross Sections at HERA*, DESY 99-056 (May 1999), The European Physical Journal C 11 (1999) 3, 427-445.

[10] ZEUS Collaboration; J.Breitweg et al., *Measurement of Dijet Photoproduction at High Transverse Energies at HERA*, DESY 99-057 (May 1999), The European Physical Journal C 11 (1999) 1, 35-50.

[11] ZEUS Collaboration; J.Breitweg et al., *Search for Contact Interactions in Deep Inelastic $e^+p \rightarrow e^+X$ Scattering at HERA*, DESY 99-058 (May 1999) accepted by the European Physical Journal, MS 000121.

[12] ZEUS Collaboration; J.Breitweg et al., *Measurement of High Q^2 Charged-Current e+p Deep Inelastic Scattering Cross Sections at HERA*, DESY 99-059 (July 1999), accepted by the European Physical Journal C, MS 991030.

[13] ZEUS Collaboration; J.Breitweg et al., *Angular and Current-Target Correlations in Deep Inelastic Scattering at HERA*, DESY-99-063 (May 1999), The European Physical Journal C 12 (2000) 1, 53-68.

[14] ZEUS Collaboration; J.Breitweg et al., *Measurement of D^{*+-} production and the charm contribution to F_2 in deep inelastic scattering at HERA*, DESY 99-101 (July 1999), The European Physical Journal C 12 (2000) 1, 35-52.

[15] ZEUS Collaboration; J.Breitweg et al. *Measurement of the Spin-Density Matrix Elements in Exclusive Electroproduction of ρ^0 Mesons at HERA*, DESY 99-102 (July 1999), accepted by the European Physical Journal, MS 000246.

[16] ZEUS Collaboration; J. Breitweg et al., *Measurement of diffractive photoproduction of vector mesons at large momentum transfer at HERA*, DESY 99-160 (October 1999), submitted to the European Physical Journal.

[17] ZEUS Collaboration; J. Breitweg et al., *Measurement of inclusive prompt photon photoproduction at HERA*, DESY 99-161 (October 1999), accepted by Physics Letters B - PLB 15449 / WI 5057.

[18] ZEUS Collaboration; J. Breitweg et al., *Measurement of the E_T^2,jet / Q^2 dependence of forward jet production at HERA*, DESY 99-162 (October 1999), accepted by Physics Letters B - WI 5058.

[19] J.M.Butterworth, V.A.Khoze, W.Ochs, *Soft Particle Emission Accompanying Dijet Photoproduction*, J.Phys. G25 (1999) 1457-1460.

[20] J.E. Cole, *Recent Experimental Results in Heavy Flavour Production at HERA*, J. Phys. G: Nucl. Part. Phys. 25 (1999) 1371-1376.

[21] M.E.Hayes, M.Kramer, *Heavy-Flavour Production at HERA*, J.Phys. G25 (1999) 1477-1493.

[22] K.R. Long et al., *High Q2 Deep Inelastic Scattering at HERA*, J. Phys. G: Nucl. Part. Phys. 25 (1999) 1387-1409.

[23] A. Quadt et al., *The Design and Performance of the ZEUS CTD Second Level Trigger*, Nucl. Instr. Meth. A438 (1999) 472-501.

[24] M. Botje, *A QCD Analysis of HERA and Fixed Target Structure Function Data*, DESY 99-038 (1999), NIKHEF-99-011 (in preparation).

[25] R. P. Feynman, 'Photon-Hadron Interactions', Benjamin, N.Y. (1972).

[26] Yu. Dokshitzer et al., Rev. Mod. Phys. 60 (1988) 373.

[27] A. V. Anisovich et al., Il Nuovo Cimento A106 (1993) 547.

[28] K. Charchuła, J. Phys. G19 (1993) 1587.

[29] C. P. Fong and B. R. Webber, Phys. Lett. B229 (1989) 289;
C. P. Fong and B. R. Webber, Nucl. Phys. B355 (1991) 54.

[30] Yu. Dokshitzer, V. Khoze and S. Troyan, Int. J. Mod. Phys. A7 (1992) 1875.

[31] Ya. Azimov et al., Z. Phys. C27 (1985) 65.

[32] Yu. Dokshitzer et al., Sov. Phys. JETP 68 (1988) 1303.

[33] OPAL Collab., M.Akrway et al., Phys. Lett. B247 (1990) 617;
TASSO Collab., W. Braunschweig et al., Z. Phys. C47 (1990) 187;
TASSO Collab., W. Braunschweig et al., Z. Phys. C22 (1984) 307;
TOPAZ Collab., R. Itoh et al., Phys. Lett. B345 (1995) 335.

[34] Bank of England Quarterly Bulletin , February 1998, and references therein. The two piece normal distribution is

$$\exp\left(\frac{(\ln(1/x_p)-\mu)^2}{2\Sigma^2}(1\pm g)\right),$$

where μ and Σ are the mode and r.m.s. of the distribution respectively; g is in the range $-1. < g < 1.$ and controls the skewness of the distribution. If $\ln(1/x_p) \geq \mu$ then the sign in front of g is positive, otherwise it is negative.

[35] H. Georgi and H. D. Politzer, Phys. Rev. Lett. 40 (1978) 3.

[36] R. N. Cahn, Phys. Lett. B78 (1978) 269.

[37] G. Köpp, R. Maciejko and P. M. Zerwas, Nucl. Phys. B144 (1978) 199.

[38] A. Mendez, Nucl. Phys. B145 (1978) 199.

[39] J. Chay et al., Phys Rev D45 (1992) 46, J. Chay et al., Phys. Lett. B269 (1991) 175.

[40] M. Ahmed and T. Gehrmann, Phys. Lett. B465 (1999) 297.

[41] J. Binnewies, B.A. Kniehl and G. Kramer, Phys. Rev. D52 (1995) 4947.

[42] H.L. Lai et al., Phys. Rev. D55 (1997) 1280.

[43] S. Catani and M. H. Seymour, Nucl. Phys. B485 (1997) 291, erratum-ibid B510 (1997) 503.

[44] G. Marchesini et al., Comp. Phys. Commun. **67** (1992) 465.

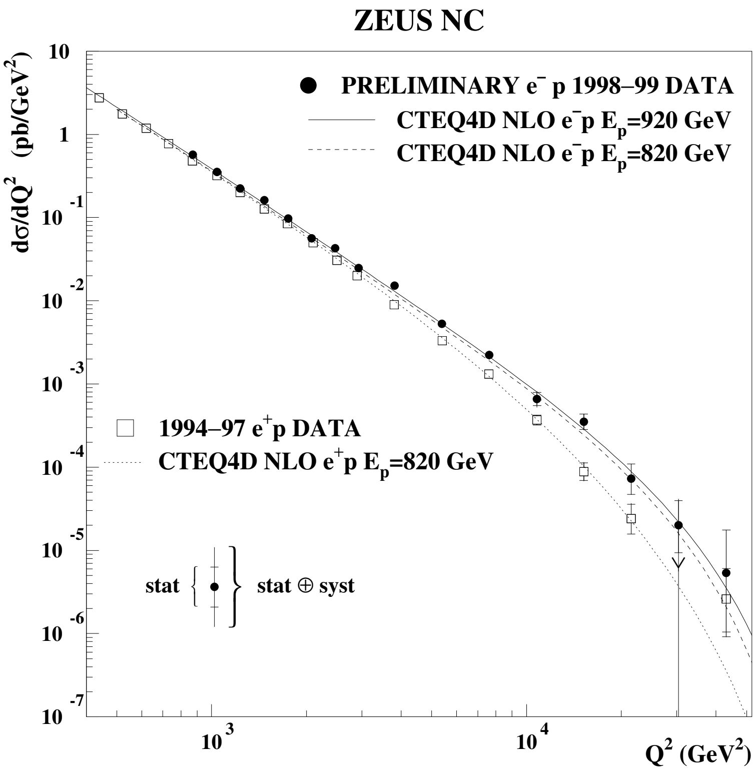

Figure 1: The high-Q^2 e^-p cross section $d\sigma/dQ^2$ (closed points) and the Standard Model predictions using the CTEQ4D parton momentum distributions at proton energies (E_p) of 920 GeV (full line) and 820 GeV (dashed line). The inner error bars (delimited by the horizontal lines) show the statistical errors, the outer ones the statistical and systematic uncertainties added in quadrature. Also shown are the ZEUS high-Q^2 e^+p data (open squares) with the corresponding SM prediction.

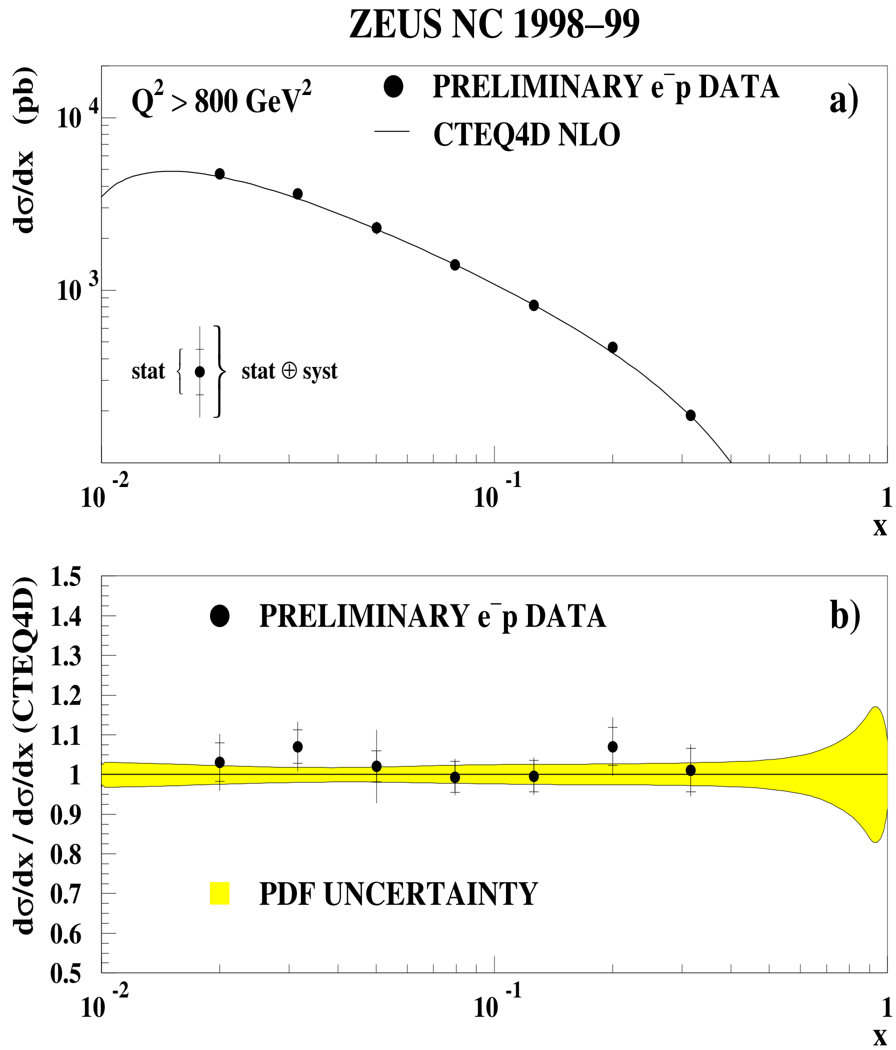

Figure 2: The high-Q^2 e^-p cross section $d\sigma/dx$ for $Q^2 > 800\,\mathrm{GeV}^2$. a) shows the ZEUS data as closed points along with the Standard Model prediction using the CTEQ4D parton momentum distributions; b) shows the ratio of the data to the Standard Model prediction using the CTEQ4D parton densities. The shaded region gives the uncertainty in the Standard Model prediction due to the uncertainty in the parton momentum distributions [24].

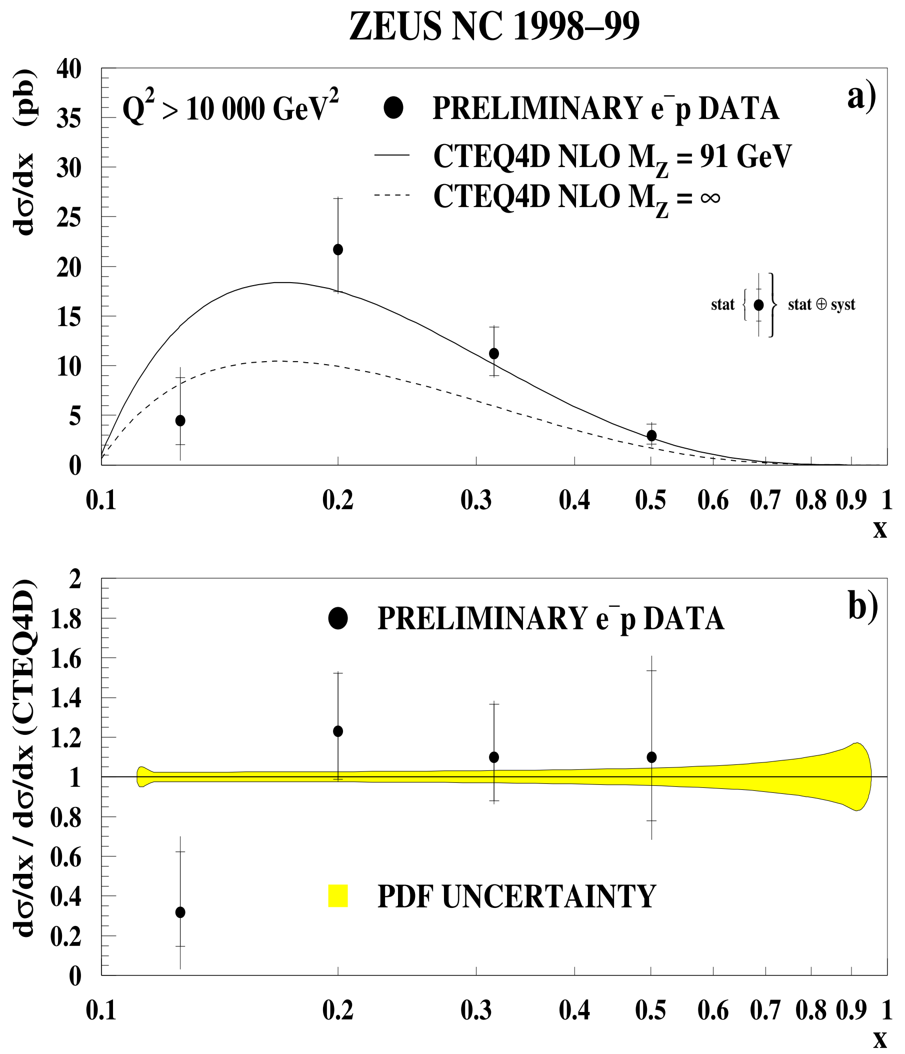

Figure 3: The high-Q^2 e^-p cross section $d\sigma/dx$ for $Q^2 > 10\,000\,\mathrm{GeV}^2$. In a) ZEUS data are shown as the closed points along with the prediction from the Standard Model using the CTEQ4D parton densities. Also shown in a) is the CTEQ4D prediction in which there is no Z^0 contribution; b) shows the ratio of the data to the Standard Model prediction using the CTEQ4D parton densities. The shaded region gives the uncertainty in the Standard Model prediction due to the uncertainty in the parton momentum distributions [24].

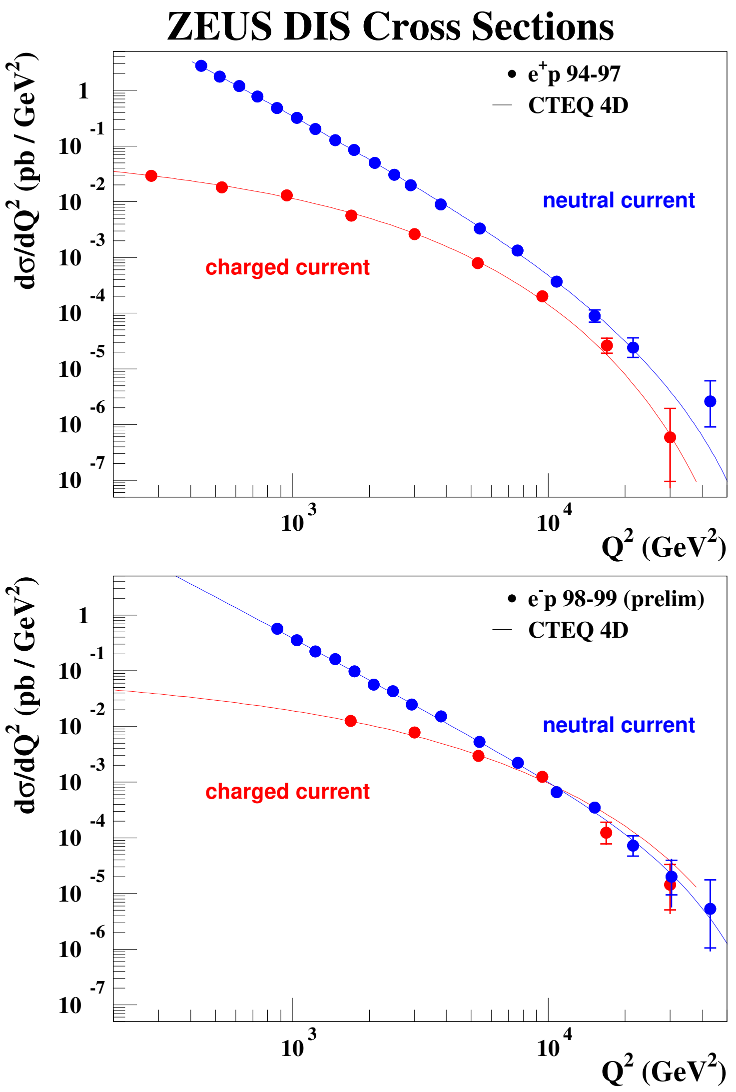

Figure 4: The high-Q^2 e^-p cross sections $d\sigma/dQ^2$ for both Neutral Current (Blue closed points), Charged Current (Red closed points) and the Standard Model predictions using the CTEQ4D parton momentum distributions for both positron (top) and electron (bottom) data.

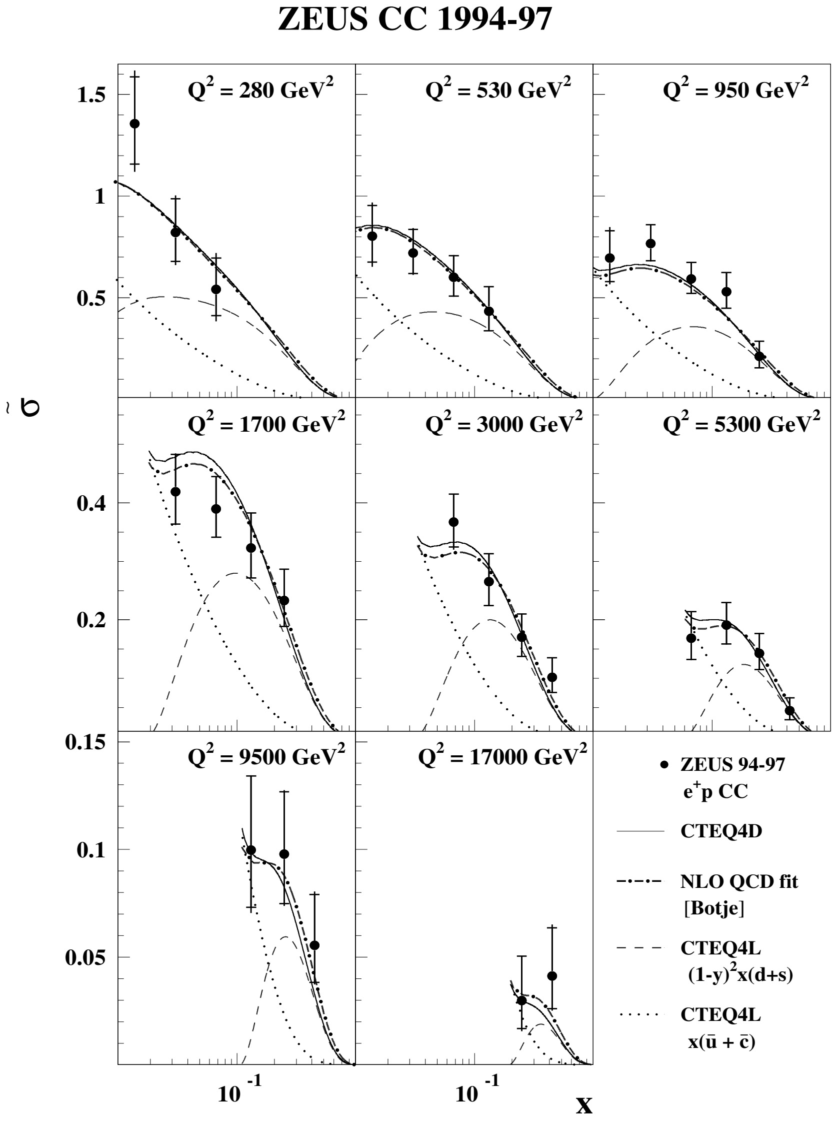

Figure 5: The reduced cross section $\tilde{\sigma}$ as a function of x, for fixed values of Q^2. The dots represent the data, while the expectations of the Standard Model evaluated using the CTEQ4D PDFs are shown as the solid lines. For illustration, the leading-order PDF combinations $x(\bar{u}+\bar{c})$ and $(1-y)^2x(d+s)$, taken from the CTEQ4L parameterization, are plotted as dotted and dashed lines, respectively. Also shown is the result of the NLO QCD fit (dash-dotted line).

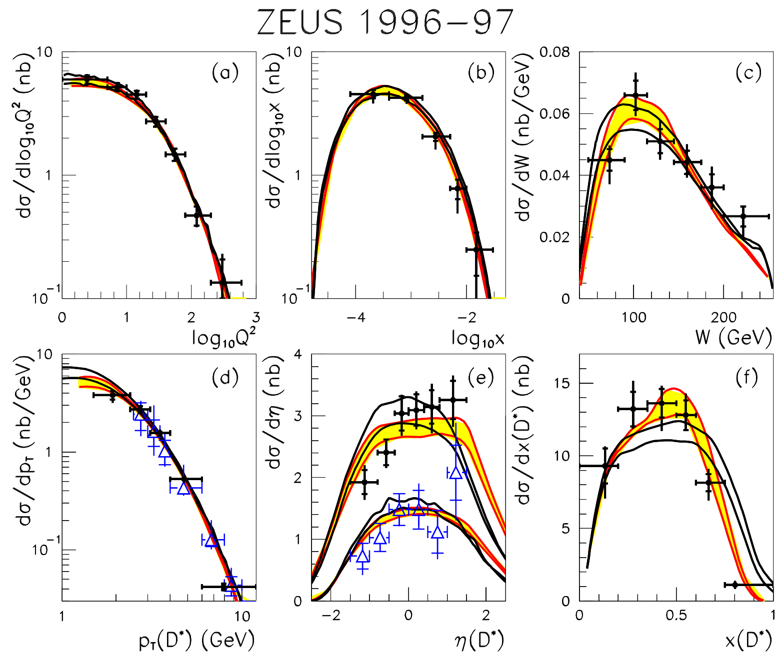

Figure 6: Differential cross sections for D^* production from the $K\pi\pi_s$ final state (solid dots) in the Q^2, y, P_{tD^*} and η_{D^*} kinematic region as functions of (a) $log(Q^2)$, (b) $log(x)$, (c) W, (d) P_{tD^*}, (e) η_{D^*} and (f) x_{D^*}. The inner error bars show the statistical uncertainties while the outer ones show the statistical and systematic uncertainties summed in quadrature. The results from the Kpppps channel (open triangles) are also shown in the P_{tD^*} (d) and η_{D^*} (e) plots. The data are compared with the NLO QCD calculation as implemented in HVQDIS using the ZEUS NLO pdf's. The open band corresponds to the standard Peterson fragmentation function with the parameter $\epsilon = 0.035$. For the shaded band, the Peterson fragmentation was replaced by that extracted from the RAPGAP Monte Carlo. The boundaries of the bands correspond to charm mass variations between 1.3 (upper curve) and 1.5 GeV (lower curve). In (a) and (b), the open band is indistinguishable from the shaded band.

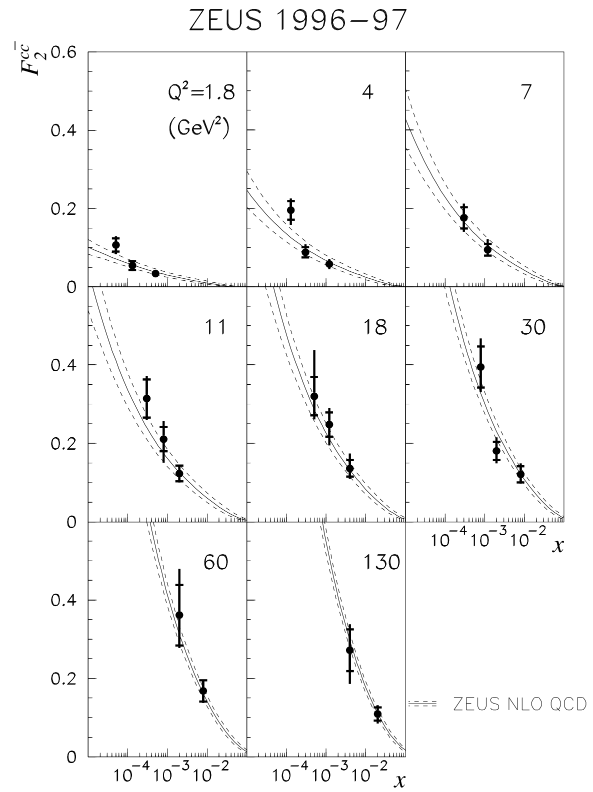

Figure 7: The measured F_2^{charm} at Q^2 values between 1.8 and 130 GeV^2 as a function of x. The inner error bars show the statistical uncertainty and the outer ones show the statistical and experimental systematic uncertainties summed in quadrature. The curves correspond to a NLO QCD calculation using the result of the ZEUS NLO QCD fit to F_2 [24]. The solid curves correspond to the central values and the dashed curves give the uncertainty due to the parton distributions from the ZEUS NLO fit.

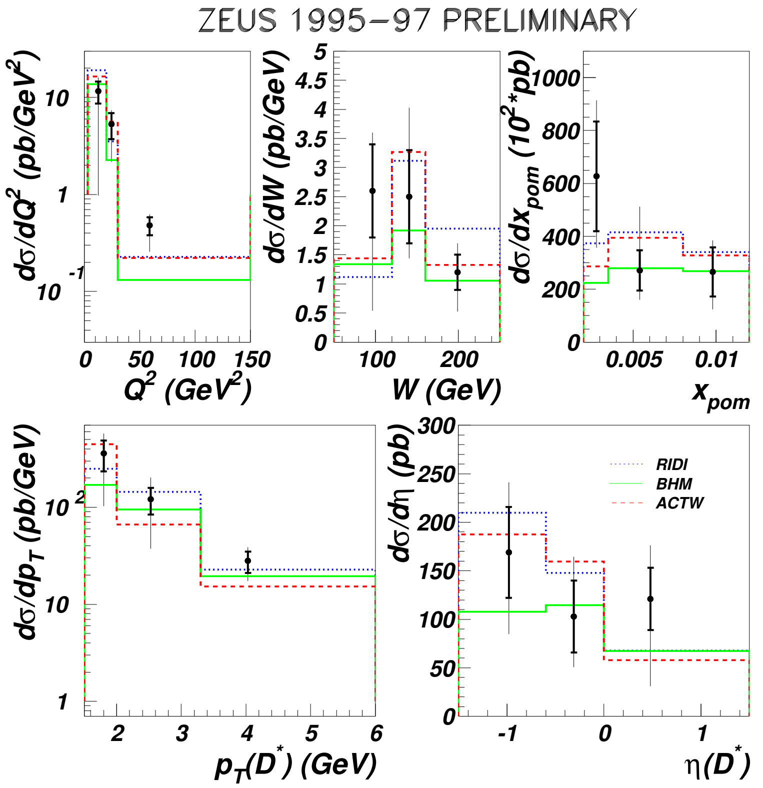

Figure 8: The differential diffractive D^{*} cross sections for the $K\pi\pi_s$ final state verses Q^2, W, xpom, $P_{tD^{*}}$ and $\eta_{D^{*}}$ in the kinematic range selected. The points show the data with the inner error bars showing the statistical uncertainty and the total bar the statistical and systematic uncertainties summed in quadrature. The bin width over which the differential cross sections were averaged are indicated by the binning of the predictions from the different models used for comparison.

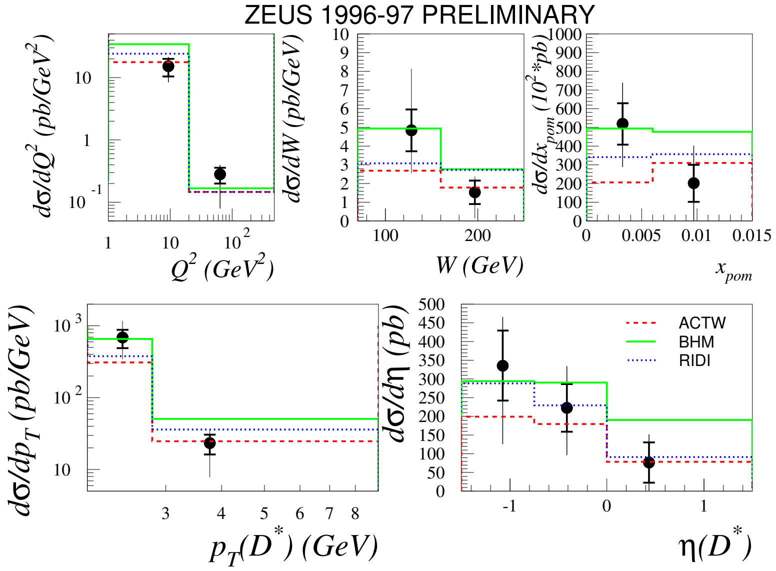

Figure 9: The differential diffractive D^* cross sections for the $K\pi\pi\pi\pi_s$ final state verses Q^2, W, xpom, P_{tD^*} and η_{D^*} in the kinematic range selected. The points show the data with the inner error bars showing the statistical uncertainty and the total bar the statistical and systematic uncertainties summed in quadrature. The bin width over which the differential cross sections were averaged are indicated by the binning of the predictions from the different models used for comparison.

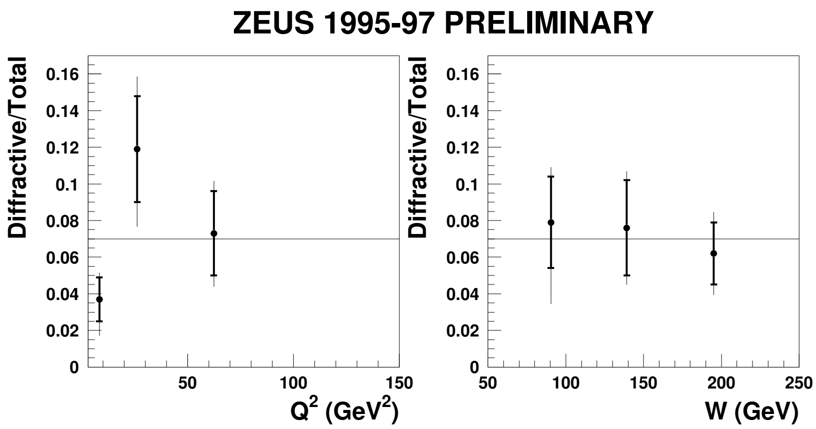

Figure 10: The ratio of diffractively produced D_s^* to total D_s^* in the kinematic range selected. The left figure shows the ratio verses Q^2 and the right plot the ratio verses W. The inner error bars indicate the statistical uncertainty and the total bar the quadratic sum of the statistical and systematic errors.

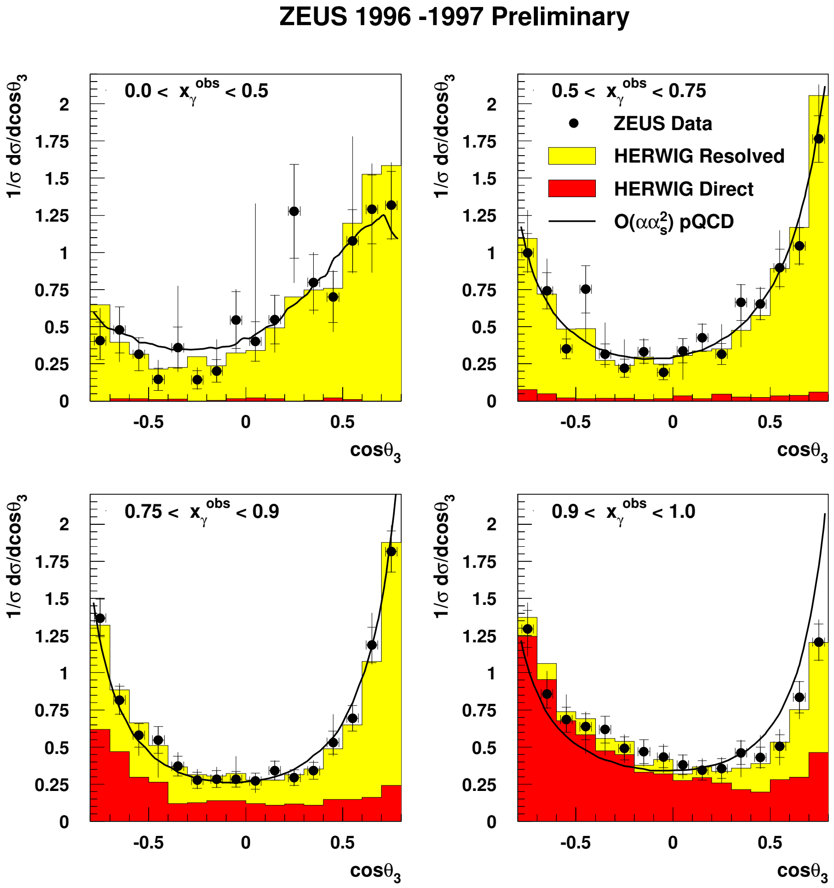

Figure 11: Three jet cross sections at HERA. LO resolved photon processes are shown as red, and LO direct as yellow.

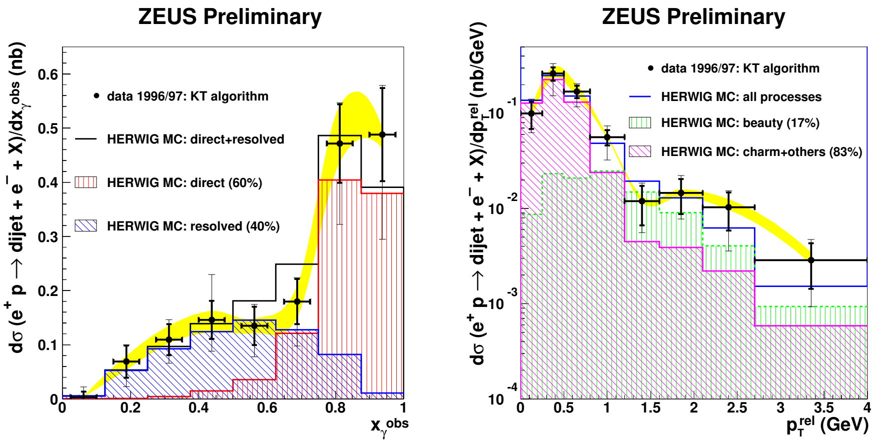

Figure 12: (a) The x_γ^{OBS} distribution for heavy flavour decays tagged with an electron, confirming the presence of a resolved component. (b) The transverse momentum of the electron relative to the jet axis, showing the presence of beauty quarks.

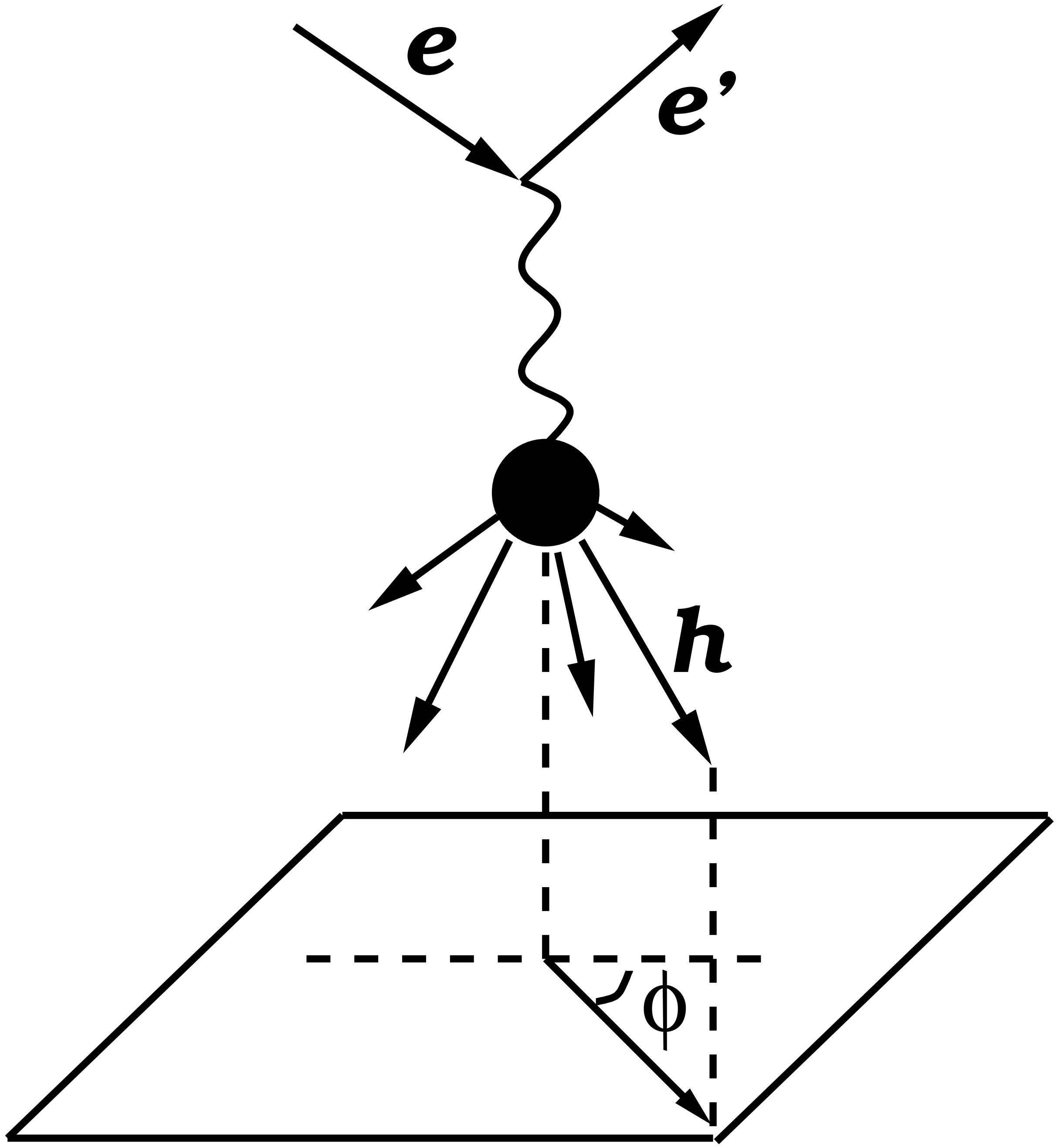

Figure 13: Definition of the azimuthal angle ϕ.

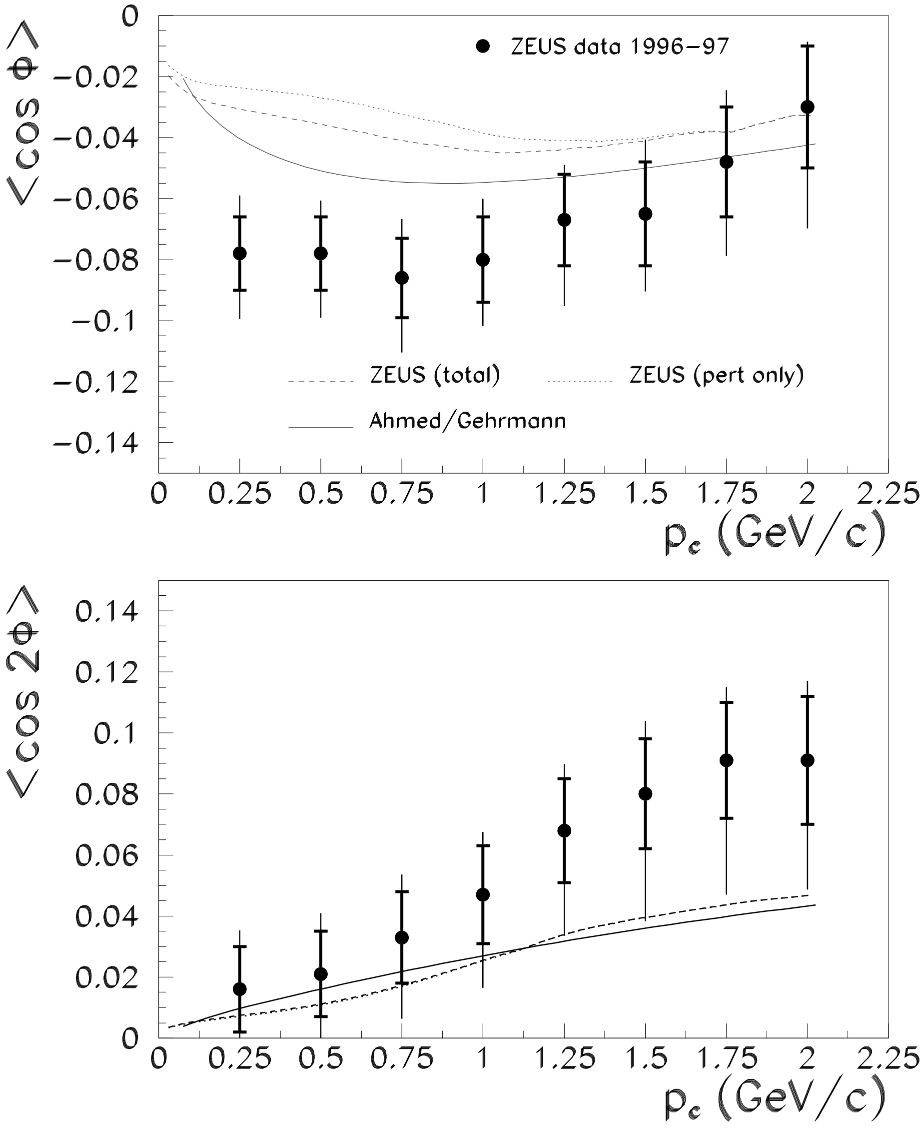

Figure 14: The data points are $\langle \cos\phi \rangle$ and $\langle \cos 2\phi \rangle$ as a function of p_c in the kinematic region $0.01 < x < 0.1$ and $0.2 < y < 0.8$ for charged hadrons with $0.2 < z_h < 1.0$. The inner error bars are statistical errors, the outer are statistical and systematic errors added in quadrature. The lines are the LO predictions from Ahmed & Gehrmann (full line), ZEUS with perturbative and non-perturbative contributions (dashed line) and ZEUS with purely perturbative contribution (dotted line).

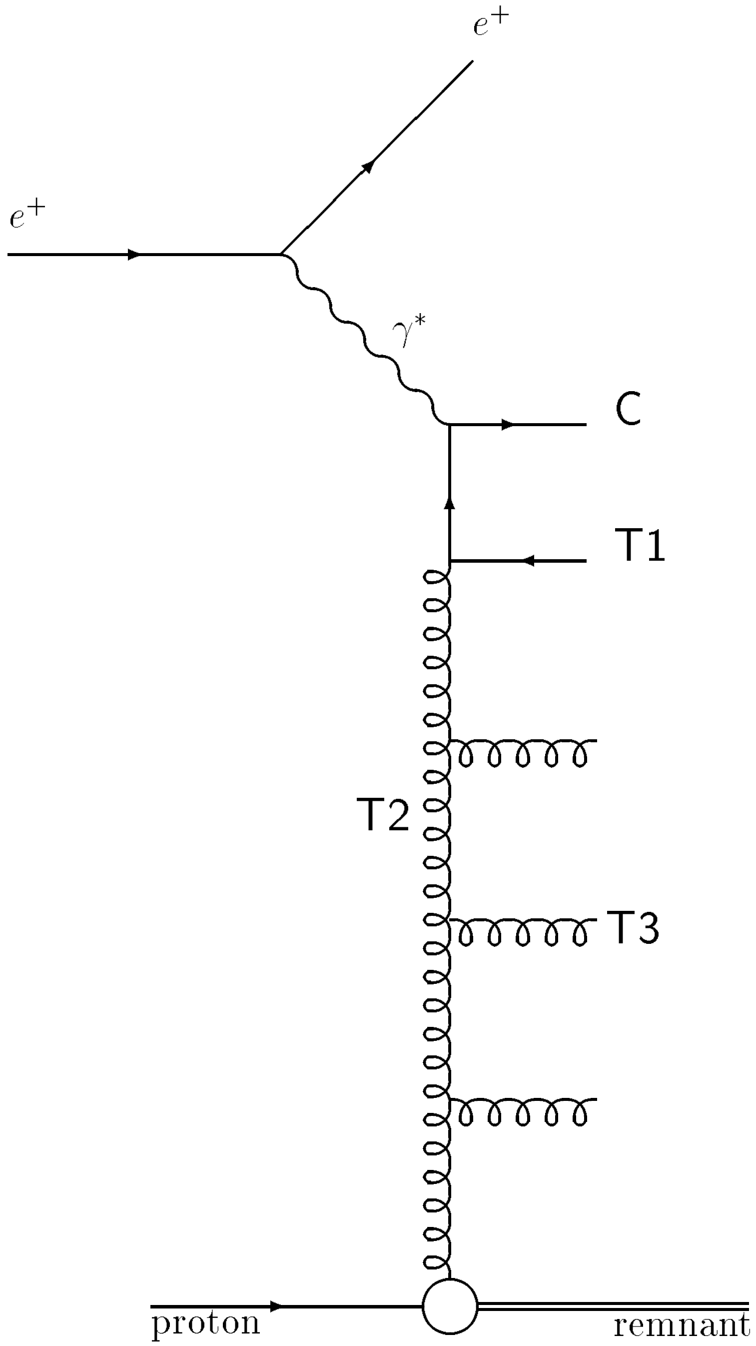

Figure 15: A schematic of DIS scattering at low x within the MLLA framework. Quark C represents the struck sea quark in the current fragmentation region. T1 is the other half of the quark box which is in the target region. T2 is the t-channel gluon exchange and T3 the rungs of the gluon ladder.

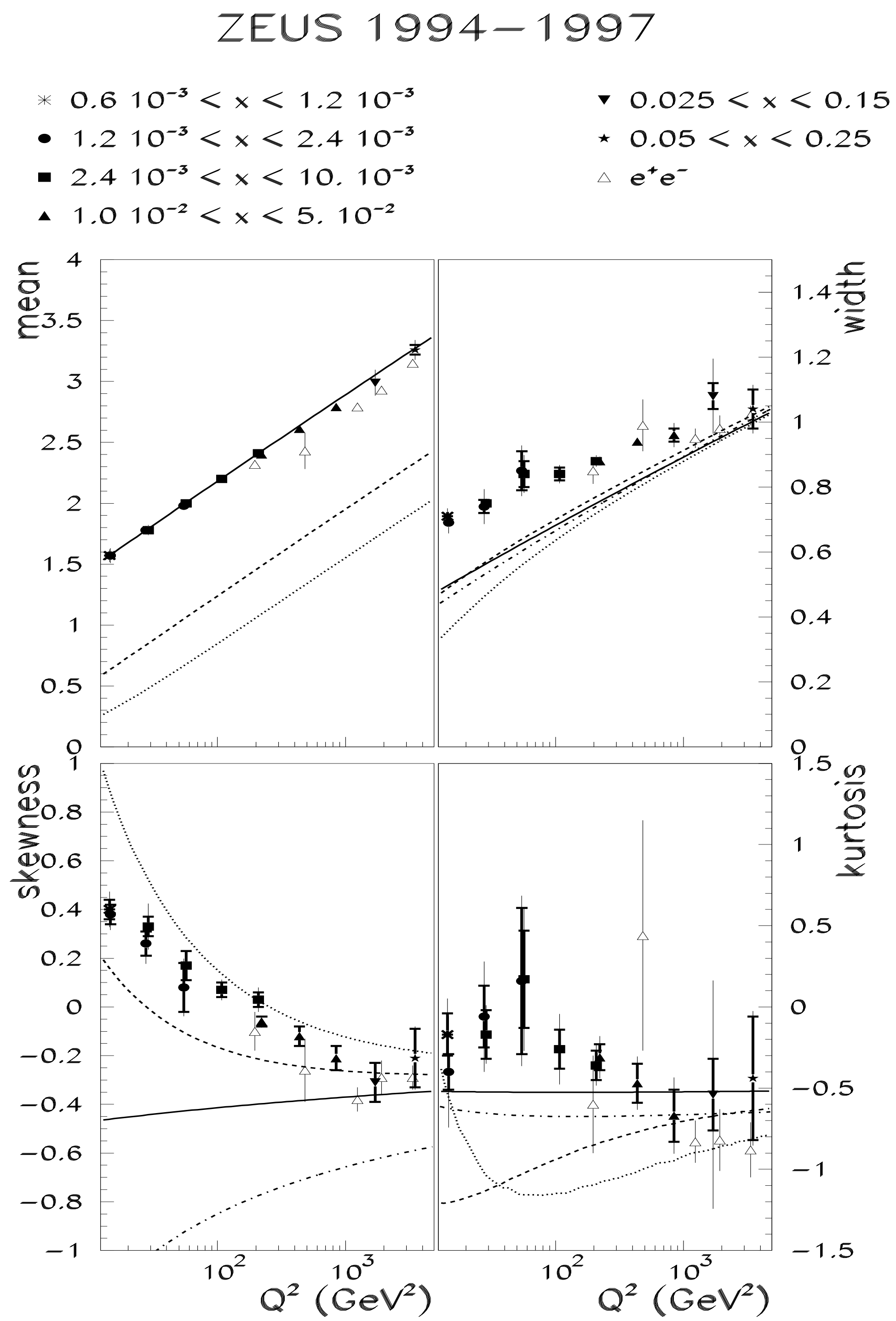

Figure 16: Evolution of the mean, width, skewness and kurtosis of the $\ln(1/x_p)$ distribution in the current fragmentation region with Q^2. Data from e^+e^- and ep are shown together with the MLLA predictions of Dokshitzer *et al* [30] (the full line is $Q_0 = \Lambda$, the dashed $Q_0 = 2\Lambda$, and the dotted $Q_0 = 3\Lambda$) and the limiting spectrum predictions of Fong and Webber [29] (dash-dotted line where available.) The overlapping points are different x ranges in the same Q^2 range. The inner error bars are the statistical error and the outer error bars are the systematic and statistical errors added in quadrature.

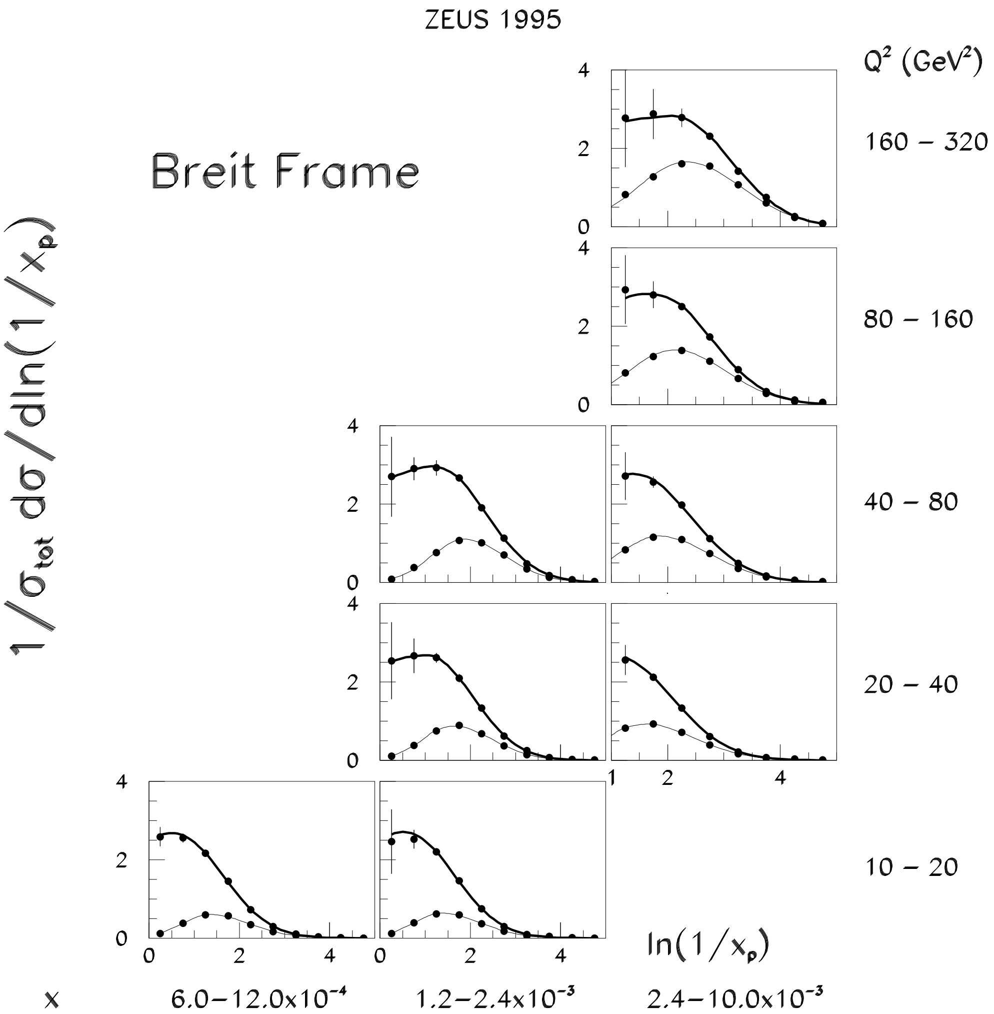

Figure 17: The corrected $\ln(1/x_p)$ distributions for the target and current regions for the 1995 data. Fitted two-piece normal distributions are shown to guide the eye. The heavy line corresponds to the target region, the light line to the current region. The error bars are the sum of the statistical and systematic errors in quadrature.

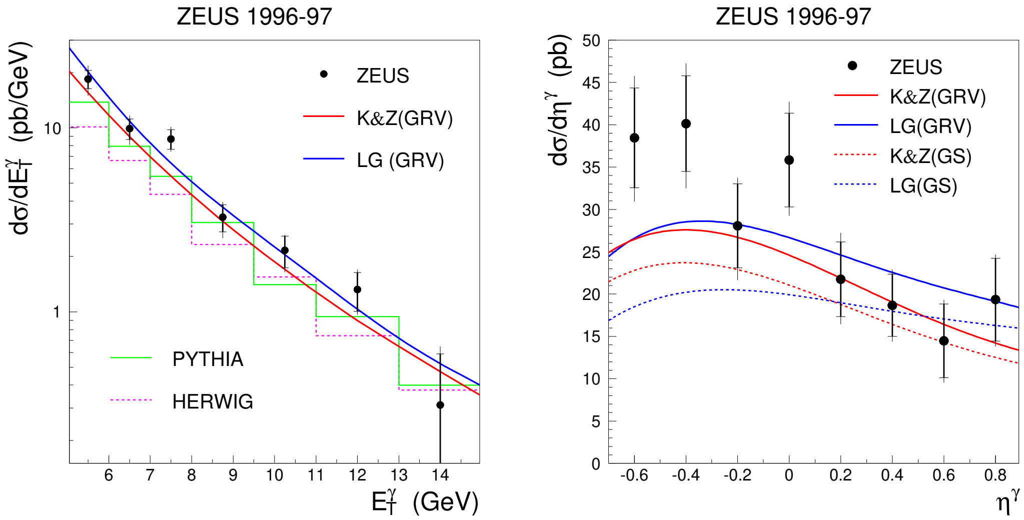

Figure 18: (a) The first plot shows the transverse component of the energy of the prompt photons observed by ZEUS compared with the theoretical predictions. (b) The second plot shows the angular distribution of the prompt photons plotted against rapidity, again compared with theoretical predictions.